Progress in Natural Science: Materials International 29 (2019) 341–348

HOSTED BY

Contents lists available at ScienceDirect

Progress in Natural Science: Materials International

journal homepage: www.elsevier.com/locate/pnsmi

Original Research

High-throughput modeling of atomic diffusion migration energy barrier of fcc metals

Yuchao Feng[a,b,1], Min Liu[a,b,1], Yongpeng Shi[a,b], Hui Ma[a], Dianzhong Li[a], Yiyi Li[a], Lei Lu[a], Xingqiu Chen[a,*]

[a] Shenyang National Laboratory for Materials Science, Institute of Metal Research, Chinese Academy of Sciences, Shenyang 110016, China
[b] School of Materials Science and Engineering, University of Science and Technology of China, Shenyang 110016, China

ABSTRACT

In crystalline solids, to computationally determine atomic migration energy barrier is a highly time consuming challenge within the framework of Density Functional Theory (DFT). Through first-principle calculations, here we have proposed a simple, high-throughput formula to fast, effectively calculate atomic migration energy barrier for fcc metals through three basic parameters of materials, the equilibrium volume (V_0), the bulk modulus (B_0) and the Poisson's ratio (ν). This formula is useful not only for the ideal strain-free lattices but also for the uniaxially strained lattices. It has been further validated by a series of fcc metals when compared with both available experimental or theoretical data and DFT-derived data obtained by Nudged Elastic Band (NEB) method. Moreover, we have investigated the effect of uniaxial deformation on the diffusion behavior of vacancy in fcc metals. Our calculations revealed that in fcc metals under uniaxial tensile deformation, vacancy prefers to diffuse along the direction that is perpendicular to the uniaxial tensile deformation.

1. Introduction

Ions diffusion is responsible for many different materials processes [1]. Generally, there are two main mechanisms for atomic diffusion in crystalline solid, the vacancy mechanism and interstitial mechanism. In the self-diffusion in monoatomic close-packed crystals, the vacancy mechanism is the most common and dominant means of atomic diffusion [2]. In various metals, all elements self-diffusion usually proceeds via vacancy-mediated mechanism. Vacancy inevitably occurs in materials, when the temperature goes higher above the absolute zero. The self diffusion of atoms would hence largely affect the physical, chemical and mechanical properties of materials, such as, light-admitting quality, ductility, creep, fracture, oxidation and corrosion, as well as electronic and transport properties, and so on [3]. Mechanically, the vacancy-mediated self diffusion can be mostly considered as a thermally activated process, in which a migrating atom passes through an energy barrier and moves from a local energy minimum site to an adjacent vacant site [4]. Conceptually, the self diffusivity in a given material is determined by the basic processes of both the vacancy formation and the vacancy migration. Accordingly, the self-diffusion activation energy ΔH_v^q is a sum of the vacancy formation energy H_v^f and the vacancy migration energy H_v^m [5,6]. Despite of extensive experimental and computational efforts that had been made to obtain the values of both H_v^f and H_v^m [3,7–12], it is extremely challenging to fast and effectively obtain these values. This challenge stems from the mutual interactions between vacancy and other types of defects, while highly scattered and limited data measured by experiments [7,11].

In comparison with the experiments, first-principles calculations within the framework of Density-Functional Theory (DFT) have been proved a good way in deriving the values of both H_v^f and H_v^m [3,10–12]. The key factor is to search for the transition state (TS) [13,14]. Once one determines the initial and final positions of the vacancy in the supercell method, the Nudged Elastic Band (NEB) [15,16] method is commonly used to seek the minimum energy path between the initial and final configurations for a specified atom jump. The NEB method is successful in determining the vacancy migration energy H_v^m by using spring-like force acting on the unstable atom while looking at intermediate steps along the diffusion path, called images. Through this common NEB method, accurate diffusion activation energies for self-diffusion in fcc, bcc, and hcp metals are successfully calculated. For instance, in an early study of Angsten et al. [11] both H_v^f and H_v^m of a series of fcc and hcp elemental solids were reported. Most recently, both H_v^f and H_v^m for 82 pure elemental solids in the periodic table in bcc, fcc and hcp structures have been calculated by Shang et al. [3].

Although the great success for first-principles calculations has been achieved, there are still two notable limitations for the calculations of H_v^m. Firstly, the calculations of diffusion within a NEB framework of DFT are highly complex and time consuming. Secondly, to our best

* Corresponding author.
E-mail address: xingqiu.chen@imr.ac.cn (X. Chen).
[1] Yuchao Feng and Min Liu contributed equally.

https://doi.org/10.1016/j.pnsc.2019.02.007
Received 25 February 2019; Accepted 26 February 2019
Available online 22 April 2019

knowledge, those previous calculations for diffusion activation energies all refer to the ideal strain-free equilibrium states of materials. Nevertheless, for most materials ranging from structural or functional materials to devices, when they are under service it is inevitable for them to have deformation occurred. Considering the importance of understanding the effect of deformation on vacancy, a number of theoretical and experimental studies have been performed to investigate vacancy behaviors under various deformations [17–25]. However, most of those works focused on the behaviors of vacancies, including their formation, annihilation and migration, as well as interactions with other types of defects. To date no any investigation has been directly related to the atomic diffusion migration energy barriers under deformations.

Within this context, through first-principles calculations, we have developed a fast, effective and high-throughput modeling of calculating the diffusion migration energy barrier in stable and metastable fcc metals for both ideal strain-free lattices and uniaxially strained lattices under deformations via three basic parameters of materials: the equilibrium volume (V_0), the bulk modulus (B_0) and the Poisson's ratio (ν). The validity of this modeling has been confirmed by comparing with both available experimental data and DFT-NEB-derived data. In addition, we have elucidated the crucial diffusion process of fcc metals under uniaxial tensile deformation, revealing that under uniaxial strains the vacancy prefers to diffuse at the direction perpendicular to the tensile deformation.

2. Methodology and computational details

Within the framework of Density Functional Theory (DFT) [26,27] using Vienna Ab-initio Simulation Package (VASP) [28,29], we have simulated the vacancy diffusion of a series of ground-state stable and metastable fcc metals under uniaxial tensile deformation. We have adopted the projector augmented wave (PAW) [30] method and generalized gradient approximation (GGA) within the Perdew-Burke-Ernzerh of (PBE) [31] exchange-correlation (X-C) function. A very accurate optimization of structural parameters was achieved by minimizing forces (below 0.0001 eV/Å) and the cut-off energies of plane wave were assigned for each element at 1.5 times the maximum energy cutoff in the PAW potential file (denoted ENMAX). A 15 × 15 × 15 k-mesh grid generated by the Monkhorst-Pack scheme was used to sample the Brillouin zone. The spin-polarization calculations have been performed for both ferromagnetic fcc Ni and metastable fcc Co metals. Nevertheless, only nonmagnetic state has been considered for fcc Fe because fcc Fe is paramagnetic [32]. In order to simulate atomic diffusion under the uniaxial deformation, we have built a 3 × 3 × 3 supercell. In Fig. 1, the force loading direction is illustrated along the *b* axis for the uniaxial tensile deformation. Before the diffusion calculations, we optimized the lattice structure under different degree of uniaxial strains, via such a strategy that the *b*-axis direction of the stretched lattice was not allowed to be relaxed, whereas the other two *a*- and *c*-axis directions are free to be relaxed. In particular, it needs to be emphasized that during the tensile deformation of our current computations, we assume that the lattices will remain in an elastic deformation without the occurrence of any plastic deformations. The optimized results commonly demonstrated that along the *b* axis the supercell is stretched, whereas both that *a* and *c* axes get slightly shorter in comparison with ideal strain-free case (see details in Supplementary Material). At each uniaxial strain, the vacancy formation energy of H_v^f was defined as the energy difference between the monovacancy-containing (H_{N-1}) and ideal vacancy-free (H_N) supercells, as expressed in $H_v^f = H_{N-1} - \frac{N-1}{N}H_N$ (here, *N* is the number of atoms in the supercell). To calculate the diffusion process, we have considered all possible migration paths for vacancy-mediated atom migrating to its first nearest neighboring (1nn) and the second nearest neighboring (2nn) positions. The former is labeled as the *P1* path and the latter is labeled as the *P2* path (see Fig. 1). It should be noted that for ideal strain-free lattice, both *P1* and *P2* paths are just identical as migration paths to its 1nn position. However, when fcc metals are under uniaxial tensile deformation, *P1* and *P2* are no longer the same. The distance of *P2* is slightly longer than that of *P1* because of the deformation. The *P1* path is strictly perpendicular to the direction of the uniaxial tensile deformation, whereas the *P2* path is along the uniaxial tensile direction. Here, we have considered six different strains of uniaxial tensile deformation from 0% to 5% with an interval step of 1%. Under each strain, we simulated these two different diffusion migration paths (*P1* and *P2*) using the NEB method.

3. Results and discussions

Table 1 shows the calculated vacancy formation energies (H_v^f) and vacancy migration energy barriers (H_v^m) for 24 ground-state stable or metastable fcc metals at their ideal strain-free equilibrium states along with pervious DFT-derived data and available experimental values from the Landolt-Börnstein New Series [7]. For both H_v^f and H_v^m of all selected 24 fcc metals, our calculated values are in good agreement with previous DFT-derived data [3,11] and available experimental data [7] with an exception of fcc Th metal. From Table 1, it can be seen that the largest deviations for both H_v^f and H_v^m occurs in Th, when compared with its experimental data. First of all, it needs to be emphasized that our current DFT-derived H_v^f value of 2.27 eV and the DFT-NEB-derived H_v^m value of 1.05 eV are in the nice agreement with previously DFT-derived H_v^f of 2.19 eV, 1.92 eV and 2.10 eV [3,11,33] and previous DFT-NEB-derived H_v^m of 1.13 eV and 1.25 eV [3,11], respectively. In the second, no matter what theoretical methods of the currently DFT calculations in this work or in the previous theoretical works [3,11,33] were used, the theoretical values for both H_v^f and H_v^m had over 50% deviations, when compared with the early experimental data for fcc Th. It is clear that the currently DFT-derived vacancy formation energy (H_v^f = 2.27 eV) is much higher by over 50% than the early experimental data (1.08 eV–1.48 eV and 1.28 ± 0.23 eV [7,34]), whereas the DFT-NEB-derived vacancy migration energy barrier (H_v^m = 1.05 eV) is much lower by over 50% than the early experimental estimation of 2.04 eV and 2.08 ± 0.23 eV [7,34]. More recently, through a norm-conserving Troullier-Martins pseudo potential combined with the DFT-NEB method, the vacancy migration energy barrier for fcc Th is calculated as 0.75 eV [33], showing a much larger deviation from the early experimental data [7,34]. The reasons for the deviations between the DFT-derived data and experiments for fcc Th could be twofold. Firstly, the deviations were thought to be ascribed to the employed X-C functions on simulations [35–37]. For instance, Th metal has strongly correlated *f* electronic states which can not be treated correctly through conventional DFT calculations. The computational methods beyond the conventional DFT calculations are necessary for the Th metal. Secondly, the experimental methodologies and the purity of samples may also be the possible reason for these deviations [3]. The early experimental sample of Th, which was used for the experimental measurement of the diffusion activation energy (3.36 eV) in 1975 [38], was further used in 1984 to obtain the vacancy formation energy (1.28 ± 0.23 eV) by the positron annihilation measurement [34]. However, this sample was reported to contain less than 0.005 at.% of carbon, nitrogen, and oxygen impurities [34,38], and these impurities definitely affected the experimental accuracy.

Table 2 summarizes the H_v^f for 24 fcc metals under a uniaxial strain from 0% to 5%. For Ag, Al, Au, Fe, Hf, Ir, Li, Mg, Na, Ni, Pb, Pd, Pt and Ru, the H_v^f with a uniaxial strain is slightly increased, compared with the ideal strain-free equilibrium states. This fact indicates that in those fcc metals, it is a bit more difficult to have vacancy occurred when uniaxial tensile deformation is applied. However, the situation is different for other fcc metals of Ca, Co, Cu, Ho, Re, Sc, Tb, Th, Ti and Zr. The lowest H_v^f is no longer at 0%. For Ca, Co, Ho, Re, Tb, Th, Ti and Zr the lowest H_v^f is at 5%, for Cu at 4% and for Sc at 3%.

Table 3 summarizes the H_v^m values for migration energy barriers along both *P1* and *P2* paths of 24 fcc metals with a uniaxial strain from

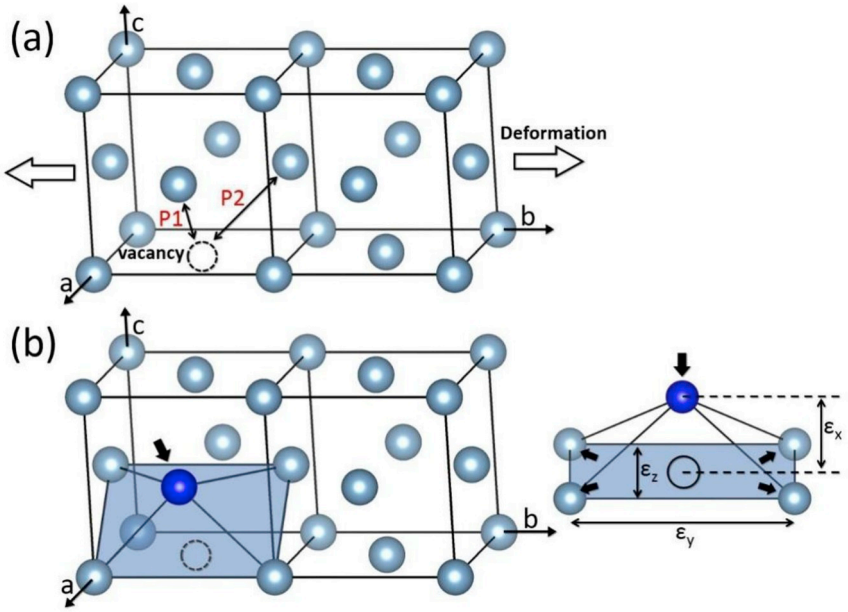

Fig. 1. Schematic diagram of (a) fcc metals under uniaxial tensile deformation, and (b) vacancy-mediated self-diffusion atom migrating from IS to TS.

Table 1
DFT-derived vacancy formation energy (H_v^f in eV) and vacancy migration energy (H_v^m in eV) for 24 selected fcc metals.

Metals	H_v^f			H_v^m		
	This work	Previous DFT	Expt.	This work	Previous DFT	Expt.
Ag	0.83	0.79, 0.68	1.06–1.18	0.63	0.59, 0.70	0.55–0.86
Al	0.62	0.63, 0.61	0.60–0.80	0.62	0.57, 0.58	0.55–0.70
Au	0.52	0.39, 0.40	0.89–1.02	0.62	0.67, 0.53	0.62–0.94
Ca	1.16	1.16, 1.13	–	0.39	0.44, 0.47	–
Co	1.79	1.83, 1.79	–	1.11	1.05, 1.01	–
Cu	1.09	1.06, 1.07	0.92–1.31	0.74	0.67, 0.72	0.67–0.76
Fe	2.36	1.86, 2.32	–	1.43	—, 1.38	–
Hf	2.04	2.14, 2.09	–	0.87	0.68, 0.81	–
Ho	1.71	1.70, 1.74	–	0.91	0.68, 0.73	–
Ir	1.60	1.63, 1.55	–	2.49	2.75, 2.54	–
Li	0.61	0.61, 0.60	–	0.16	0.07, 0.16	–
Mg	0.87	0.83, 0.82	–	0.33	0.36, 0.41	–
Na	0.37	0.40, 0.38	–	0.15	0.06, 0.14	–
Ni	1.42	1.46, 1.43	1.45–1.80	1.20	1.12, 1.08	0.90–1.30
Pb	0.50	0.45, 0.45	0.49–0.62	0.62	0.50, 0.54	0.54
Pd	1.13	1.17, 1.16	1.7, 1.85	1.00	1.03, 0.95	1.03
Pt	0.64	0.63, 0.61	1.15–1.52	1.36	1.37, 1.24	1.13–1.48
Re	2.98	3.08, 2.94	–	2.42	1.83, 1.81	–
Ru	2.58	2.63, 2.51	–	2.22	2.08, 1.85	–
Sc	1.77	1.76, 2.07	–	0.72	0.56, 0.60	–
Tb	1.76	1.72, 1.75	–	0.85	0.63, 0.71	–
Th	2.27	2.19, 1.92	1.08–1.48	1.05	1.13, 1.25	2.04
Ti	1.87	1.95, 1.95	–	0.44	0.32, 0.45	–
Zr	2.01	2.08, 2.02	–	0.61	0.32, 0.50	–

Table 2
DFT-derived vacancy formation energy (H_v^f in eV) versus uniaxial strain for 24 selected fcc metals.

Strain	0%	1%	2%	3%	4%	5%
Ag	0.83	0.91	0.86	0.88	0.84	0.86
Al	0.62	0.64	0.71	0.77	0.75	0.75
Au	0.52	0.55	0.61	0.54	0.55	0.55
Ca	1.16	1.16	1.16	1.16	1.15	1.14
Co	1.79	1.80	1.80	1.79	1.78	1.76
Cu	1.09	1.14	1.08	1.09	1.08	1.12
Fe	2.36	2.37	2.39	2.39	2.39	2.38
Hf	2.04	2.04	2.07	2.08	2.08	2.06
Ho	1.71	1.72	1.72	1.72	1.71	1.70
Ir	1.60	1.65	1.68	1.69	1.70	1.69
Li	0.61	0.62	0.62	0.62	0.62	0.61
Mg	0.87	0.87	0.87	0.88	0.89	0.87
Na	0.37	0.38	0.38	0.38	0.39	0.40
Ni	1.42	1.43	1.44	1.45	1.46	1.46
Pb	0.50	0.52	0.53	0.556	0.58	0.59
Pd	1.13	1.22	1.22	1.23	1.22	1.23
Pt	0.64	0.67	0.69	0.69	0.71	0.72
Re	2.98	3.02	3.05	3.03	2.97	2.95
Ru	2.58	2.60	2.62	2.63	2.63	2.62
Sc	1.77	1.79	1.78	1.72	1.76	1.73
Tb	1.76	1.72	1.73	1.73	1.72	1.71
Th	2.27	2.28	2.28	2.27	2.25	2.23
Ti	1.87	1.87	1.86	1.85	1.85	1.84
Zr	2.01	2.01	2.01	2.00	2.00	1.98

0% to 5%. The H_v^m values are plotted as a function of uniaxial strains in Fig. 2. The filled squares represent the H_v^m for vacancy migrating in the *P1* path and the open circs correspond to the H_v^m for vacancy migrating in the *P2* path. In all 24 fcc metals, the H_v^m values along the *P1* path are obviously lower than those for *P2* as the uniaxial strain increases. This indicates that the vacancy indeed prefers to migrate perpendicularly to the direction of tensile deformation in those metals, for the *P1* path is the energetically favorable one during the migration process for all these 24 metals. To explain the phenomenon that vacancy prefers to migrate in the direction perpendicular to the tensile deformation, we calculated the differential charges density for self-migrating Al atom migrates in TS position. As shown in Fig. 3, the yellow parts represent charge gain and the blue parts represent charge loss. When the strain increased, the blue parts of *P1* path are becoming thinner, which results the weaker interatomic interaction between the migrating atom and its surrounding atoms. But for the *P2* path, the situation is just opposite, the blue parts are gradually thicker, which means stronger interaction for the migrating atom. It is intuitively to expect that stronger interaction would cause higher vacancy migration energy for atom to migrate. Therefore, this explains the reason for the vacancy migration energy in *P1* is constantly lower than *P2*.

Besides, we have noted that for all these fcc metals, the H_v^m for the vacancy migration along the *P1* path commonly exhibits a nearly linear decreasing trend against the applied strain in Fig. 2. If the linear fitting is applied along the *P1* path of each metal, the goodness of the fitting is larger than 0.95 ($R^2 > 0.95$) for all 24 fcc metals. Therefore, the strain-

Table 3
DFT-NEB-derived vacancy migration energy (H_v^m in eV) for 24 selected fcc metals.

Strain	0%	1%		2%		3%		4%		5%	
Path	P1(P2)	P1	P2	P1	P2	P1	P2	P1	P2	P1	P2
Ag	0.63	0.62	0.66	0.56	0.68	0.54	0.70	0.48	0.70	0.43	0.71
Al	0.62	0.61	0.66	0.58	0.68	0.53	0.69	0.50	0.70	0.45	0.71
Au	0.62	0.58	0.65	0.54	0.68	0.49	0.70	0.43	0.70	0.39	0.71
Ca	0.39	0.37	0.42	0.33	0.42	0.30	0.43	0.26	0.45	0.23	0.41
Co	1.11	1.05	1.16	0.97	1.17	0.89	1.16	0.81	1.14	0.74	1.14
Cu	0.74	0.72	0.80	0.68	0.82	0.64	0.85	0.58	0.85	0.52	0.84
Fe	1.43	1.37	1.47	1.30	1.49	1.24	1.49	1.17	1.49	1.10	1.48
Hf	0.84	0.83	0.91	0.79	0.94	0.75	0.96	0.72	0.97	0.66	0.95
Ho	0.91	0.86	0.93	0.82	0.95	0.77	0.95	0.73	0.95	0.68	0.93
Ir	2.49	2.34	2.59	2.17	2.62	2.00	2.63	1.81	2.60	1.63	2.54
Li	0.16	0.15	0.17	0.14	0.17	0.12	0.18	0.11	0.17	0.10	0.18
Mg	0.33	0.30	0.35	0.26	0.37	0.22	0.38	0.19	0.38	0.14	0.38
Na	0.15	0.14	0.16	0.12	0.15	0.10	0.16	0.08	0.14	0.07	0.14
Ni	1.20	1.14	1.26	1.06	1.28	0.98	1.29	0.90	1.29	0.82	1.28
Pb	0.62	0.59	0.64	0.58	0.67	0.54	0.66	0.50	0.66	0.45	0.63
Pd	1.00	0.88	1.00	0.81	1.00	0.73	1.01	0.65	1.01	0.58	1.03
Pt	1.36	1.28	1.41	1.15	1.42	1.03	1.41	0.91	1.37	0.78	1.32
Re	2.42	2.33	2.51	2.24	2.57	2.12	2.59	1.96	.53	1.80	2.40
Ru	2.22	2.09	2.26	1.96	2.27	1.84	2.25	1.73	2.23	1.61	2.18
Sc	0.72	0.69	0.74	0.65	0.77	0.60	0.78	0.55	0.77	0.51	0.77
Tb	0.85	0.82	0.88	0.78	0.90	0.74	0.91	0.70	0.90	0.66	0.91
Th	1.05	0.98	1.09	0.90	1.11	0.82	1.10	0.74	1.09	0.66	1.07
Ti	0.44	0.43	0.45	0.42	0.46	0.40	0.45	0.38	0.42	0.36	0.42
Zr	0.61	0.60	0.62	0.58	0.61	0.55	0.62	0.52	0.60	0.48	0.58

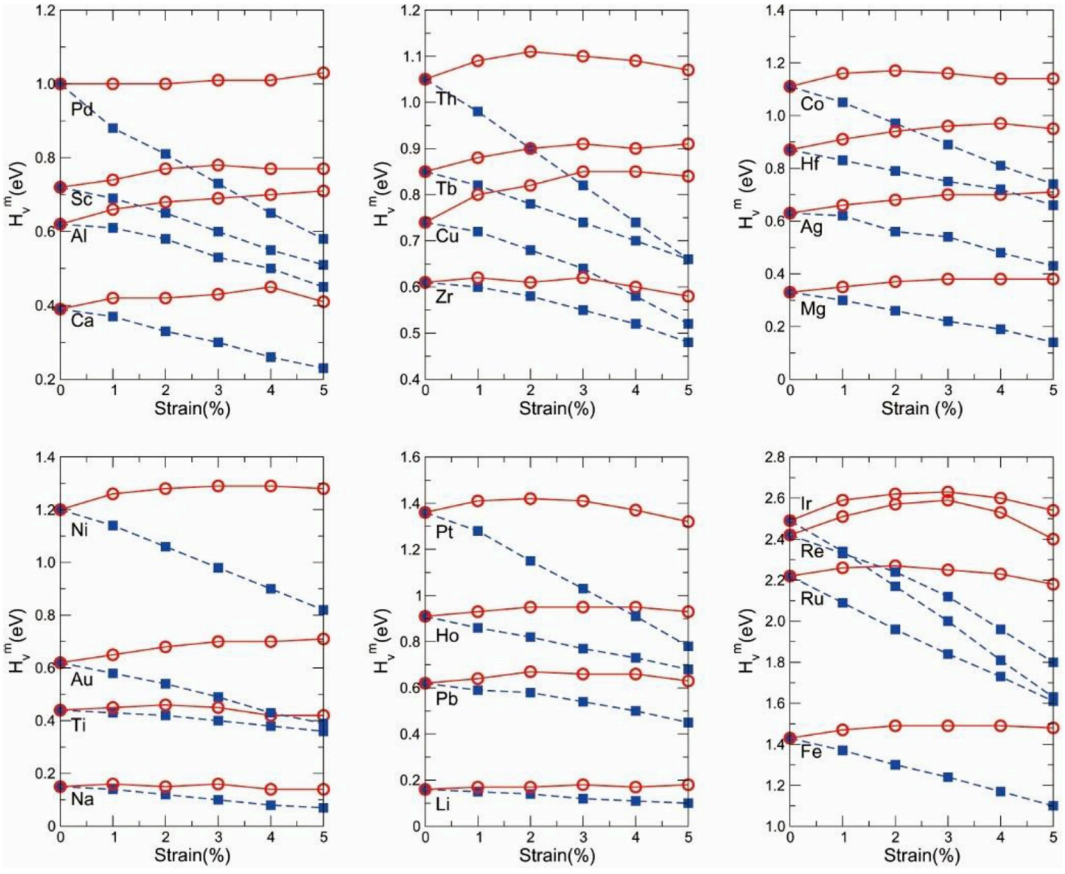

Fig. 2. The curves of H_v^m- uniaxial stain for 24 fcc metals.

dependent $H_v^m(\delta)$ along the energy-lowest *P1* path can be consistently expressed in a simple linear equation as follows,

$$H_v^m(\delta) = H_{v0}^m - k\delta \quad (1)$$

where H_{v0}^m denotes the vacancy migration energy barrier at the ideal strain-free metals. The parameter k is the fitting slope, implying the decreasing tendency of migration energy barrier with the increasing applied strain δ.

First of all, concerning the H_{v0}^m at the ideal strain-free state, different metals have highly varied values (Fig. 2). As early as in 1968, Flynn

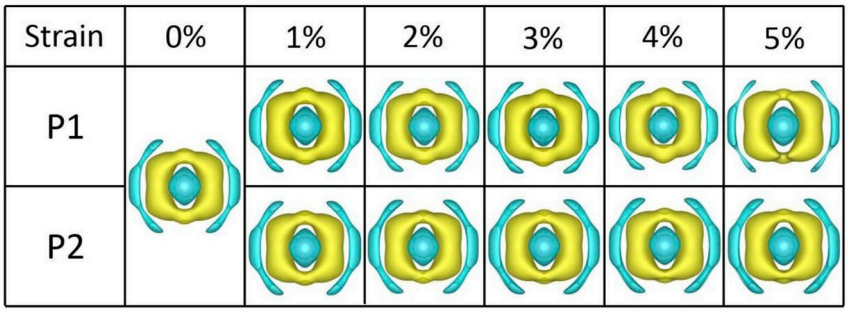

Fig. 3. Isosurfaces of differential charge density contours (0.015 e/Bohr^3) for migrating Al-atom at TS position. (Yellow: charge gain and blue: charge loss).

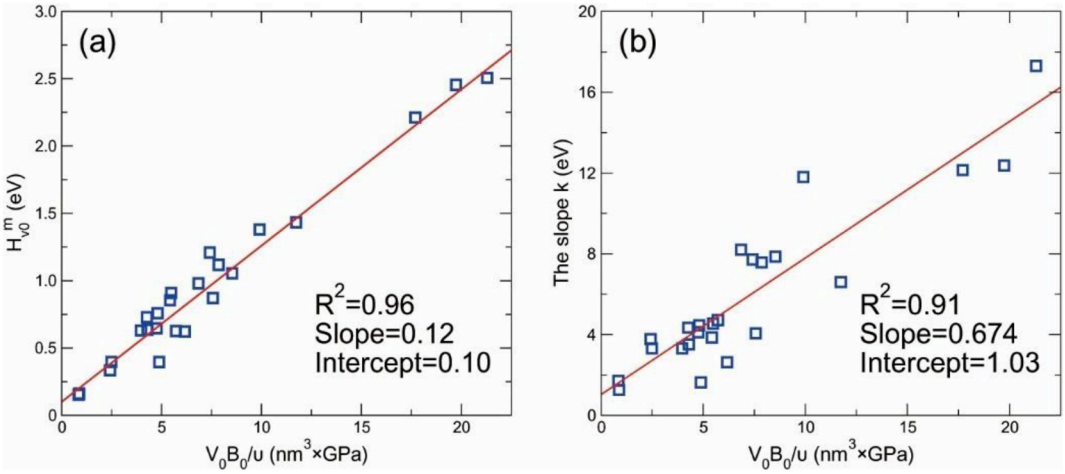

Fig. 4. (a) DFT-NEB-derived H_{v0}^m for 24 ideal strain-free fcc metals versus V_0B_0/ν, (b) slope k versus V_0B_0/ν.

Table 4
Calculated bulk modulus (B_0 in GPa), Poisson's ratio (ν) and equilibrium atomic volume (V_0 in Å^3*atom*$^{-1}$) for 24 selected fcc metals.

Metals	B_0		ν		V_0	
	This work	Expt.	This work	Expt.	This work	Expt.
Ag	94.26	103.6	0.35	0.367	17.86	17.23 [44]
Al	77.65	75.2	0.30	0.345	16.47	16.60 [45]
Au	143.82	171	0.45	0.42	18.08	16.95 [46]
Ca	17.47	17.2	0.30	0.31	42.23	43.55 [47]
Co	208.46	181.5	0.29	0.32	10.93	11.33 [48]
Cu	141.30	137.8	0.35	0.343	11.96	11.81 [46]
Fe	285.00	–	0.25	0.26	10.25	13.30 [49]
Hf	106.42	109	0.32	0.26	22.49	–
Ho	42.36	–	0.24	–	3.093	34.15 [50]
Ir	346.21	371	0.29	0.26	14.58	14.15 [46]
Li	13.75	–	0.32	0.36	20.21	20.25 [51]
Mg	35.59	35.6	0.34	0.291	23.01	–
Na	7.66	–	0.34	0.34	37.36	–
Ni	196.38	177.3	0.29	0.312	10.95	11.00 [52]
Pb	43.88	45.8	0.35	0.44	31.55	30.15 [53]
Pd	169.74	187	0.38	0.39	15.42	14.72 [54]
Pt	253.79	276	0.40	0.39	15.65	15.08 [55]
Re	376.25	34	0.29	0.26	14.95	–
Ru	306.80	286	0.24	0.25	14.00	–
Sc	51.89	–	0.30	–	24.72	–
Tb	41.31	–	0.24	–	31.93	35.15 [50]
Th	55.00	54.0	0.21	0.26	32.08	32.91 [56]
Ti	103.51	108.4	0.36	0.361	17.39	–
Zr	93.05	89.8	0.35	0.38	23.35	23.25 [57]

proposed an estimation formula $H_{v0}^m = cV_0\gamma^2$ to correlate the vacancy migration energy barrier (H_{v0}^m) to both the average elastic constant (c) and atomic volume (V_0) for fcc metals [39]. The limitation of this expression is the factor of γ^2, which has to be fitted by a product of cV_0 to the known experimental H_{v0}^m values. Using this expression, the H_{v0}^m values for only six simple fcc metals were calculated [39]. Up to 2014, Angsten et al. [11] optimized this expression by replacing the average elastic constant with the bulk modulus and further calculated the H_{v0}^m of 49 fcc stable or metastable elemental solids. However, the limitations of these two formulas are sill notable, mainly due to two-fold reason: (i) both formulas are only applied to the fcc case at the ideal strain-free condition and (ii) the low accuracy of the estimated results has restricted their further applications. For instance, compared with NEB-derived H_{v0}^m of 49 fcc candidates, the maximum derivation for the formula-generated H_{v0}^m can be as large as 0.56 eV with a rms error of 0.24 eV [11]. Inspired by their spirits [11,39], we have found that the values of H_{v0}^m for fcc candidates at the ideal strain-free condition would have much better expression by linearly correlating with a product, V_0B_0/ν, via three basic parameters of materials, the equilibrium volume (V_0), bulk modulus (B_0) and Poisson's ratio ν in Fig. 4. The details are given in Table 4. Both B_0 and ν have been calculated by using "stress-strain" approach [40,41] combined with Voigt-Reuss-Hill approximation [42,43]. The experimental data of B_0 and ν are obtained from the Smithells Metals Reference Book [8]. According these data, we have yielded a nice linear fitting between H_{v0}^m and V_0B_0/ν with a fitting goodness of $R^2 = 0.96$ for 24 fcc metals, suggesting that H_{v0}^m can be expressed as follow,

$$H_{v0}^m = 0.12 \times \frac{V_0B_0}{\nu} + 0.10 \quad (2)$$

where the units of V_0 and B_0 are nm^3 per atom and GPa,respectively, and the unit of H_{v0}^m in this equation has been converted into eV.

Secondly, concerning the slope k in Eq. (1), it mainly describes the strain-dependent migration energy barriers along the lowest-energy *P1* path for selected 24 fcc metals in Fig. 2. Interestingly, we have also found that the slope k in the Eq. (1) exhibits a nearly linear relationship

Table 5
Modeled H_{v0}^m generated by Eq. (2) for Group I (24 fcc metals, Ag – Zr) and Group II (23 fcc-structure elements, Ac –Y) compared with DFT-NEB-derived data.

	B_0	ν	V_0	Modeled H_{v0}^m	NEB data	ΔE	Expt.
Group I							
Ag	94.26	0.35	17.86	0.65	0.63	0.02	0.55–0.86
Al	77.65	0.30	16.47	0.60	0.62	0.02	0.55–0.70
Au	143.83	0.45	18.08	0.76	0.62	0.14	0.62–0.94
Ca	17.47	0.30	42.23	0.39	0.39	0.00	–
Co	208.46	0.29	10.93	1.01	1.11	0.10	–
Cu	141.30	0.35	11.96	0.66	0.74	0.08	0.67–0.76
Fe	285.00	0.25	10.25	1.46	1.43	0.03	–
Hf	106.42	0.32	22.49	0.98	0.87	0.11	–
Ho	42.36	0.24	30.93	0.74	0.91	0.17	–
Ir	346.21	0.29	14.58	2.57	2.49	0.08	–
Li	13.75	0.32	20.21	0.20	0.16	0.04	–
Mg	35.59	0.34	23.01	0.38	0.33	0.05	–
Na	7.66	0.34	37.36	0.20	0.15	0.05	–
Ni	196.38	0.29	10.95	0.96	1.20	0.24	0.9–1.3
Pb	43.88	0.35	31.55	0.56	0.62	0.06	0.54
Pd	169.74	0.38	15.42	0.89	1.00	0.11	1.03
Pt	253.79	0.40	15.65	1.25	1.36	0.11	1.13–1.48
Re	376.25	0.29	14.98	2.39	2.42	0.03	–
Ru	306.80	0.24	14.00	2.15	2.22	0.07	–
Sc	51.89	0.30	24.72	0.59	0.72	0.13	–
Tb	41.31	0.24	31.93	0.73	0.85	0.12	–
Th	55.00	0.21	32.08	1.09	1.05	0.04	2.04
Ti	103.51	0.36	17.39	0.67	0.44	0.23	–
Zr	93.05	0.35	23.35	0.82	0.61	0.21	–
Group II							
Ac	23.48	0.27	45.37	0.54	0.45	0.09	–
Ar	1.60	0.74	45.00	0.11	0.06	0.05	–
Ba	8.01	0.28	64.13	0.32	0.36	0.04	–
Be	16.96	0.15	7.88	0.8584	0.75	0.09	–
Cd	41.66	0.42	22.60	0.37	0.23	0.14	–
Ce	37.65	0.25	26.10	0.58	0.54	0.04	0.87
Cs	2.40	0.30	116.46	0.21	0.13	0.08	–
Er	16.02	0.24	40.96	0.43	0.47	0.04	–
Ga	29.64	0.47	18.91	0.24	0.18	0.06	–
He	1.60	0.40	16.54	0.11	0.02	0.09	–
In	33.65	0.45	27.33	0.35	0.23	0.12	–
K	3.20	0.35	73.60	0.18	0.016	0.02	–
Kr	0.80	0.54	57.44	0.11	0.07	0.04	–
La	24.83	0.34	37.10	0.43	0.21	0.22	–
Mn	276.38	0.24	10.73	0.46	0.65	0.19	–
Os	398.14	0.25	14.29	2.83	2.73	0.10	–
Rb	2.40	0.30	90.81	0.19	0.14	0.05	–
Rh	250.74	0.26	14.13	1.74	1.79	0.05	1.5
Sn	46.46	0.36	27.82	0.53	0.38	0.15	–
Sr	11.22	0.28	54.74	0.36	0.45	0.09	–
Tl	27.24	0.45	30.50	0.32	0.10	0.22	–
Xe	0.80	0.47	80.21	0.12	0.09	0.03	–
Y	38.45	0.27	32.35	0.6	0.67	0.01	–

with the same product of V_0B_0/ν for all fcc metals selected here, as illustrated in Fig. 4. If the k versus V_0B_0/ν data in Fig. 4b are linearly fitted, the slope k can be expressed as follows,

$$k = 0.674 \times \frac{V_0 B_0}{\nu} + 1.03 \tag{3}$$

where we have yielded a fitting goodness of $R^2 = 0.91$. By combining both Eqs. (2) and (3) into Eq. (1), the strain-dependent H_v^m can be written as follows,

$$H_v^m(\delta) = 0.12 \times \frac{V_0 B_0}{\nu} + 0.10 - \left(0.674 \times \frac{V_0 B_0}{\nu} + 1.03\right)\delta \tag{4}$$

where the parameter δ is the applied uniaxial strain. Note that here the unit of $H_v^m(\delta)$ has been converted into eV. According to Eq. (4), the strain-dependent migration energy barrier of vacancy in fcc metals can be directly derived according to the intrinsic bulk modulus B_0 and the Poisson's ratio ν, as well as its equilibrium volume V_0 at the ideal strain-free lattice.

Physically, it is highly curious as to why Eqs. (2) and (4) can reasonably predict the diffusion migration energy barriers for atom just according to macroscopic and traditional mechanical properties of materials (B_0, ν and V_0). To elucidate this mechanism, we have analyzed the results obtained by NEB calculations for each strain to find the saddle point (TS) along the lowest-energy migration *P1* path. Interestingly, the structure for atom diffusion at the TS along the *P1* path is consistent for each strain applied here. As illustrated in Fig. 1, the shadowed rectangle represents the migration window. The blue ball denotes the self-diffusion atom. When the atom migrates to the saddle point position, the diffusive atom always diffuses at the halfway of migration path and locates at the center of a rectangle shaped by its four surrounding atoms. This rectangle is the shaped area in Fig. 1b. Here, we defined this shaped rectangle as the migration window. Therefore, the value of H_v^m for *P1* is greatly correlated to the energy costing for atom migrating through this migration window. In other words, H_v^m reflects how difficult for the atom to migrate through this migration window. It has been noted that the bulk modulus B_0 can be indeed viewed as the energy density per a unit volume to reflect the average interatomic interaction bonding strength under isotropic deformation. Accordingly, the product B_0, between the bulk modulus and the equilibrium volume, refers to the energy to resist such a deformation. The larger the B_0 term is, the more difficult for the self-diffusion atom to pass through the migration window due to the stronger interatomic bonding interaction. In addition, when atom diffuses through the TS point, the migration window will experience an expansion, which causes the local deformation. We found that this behavior is related with the Poisson's ratio (ν). To elucidate it, here we first defined

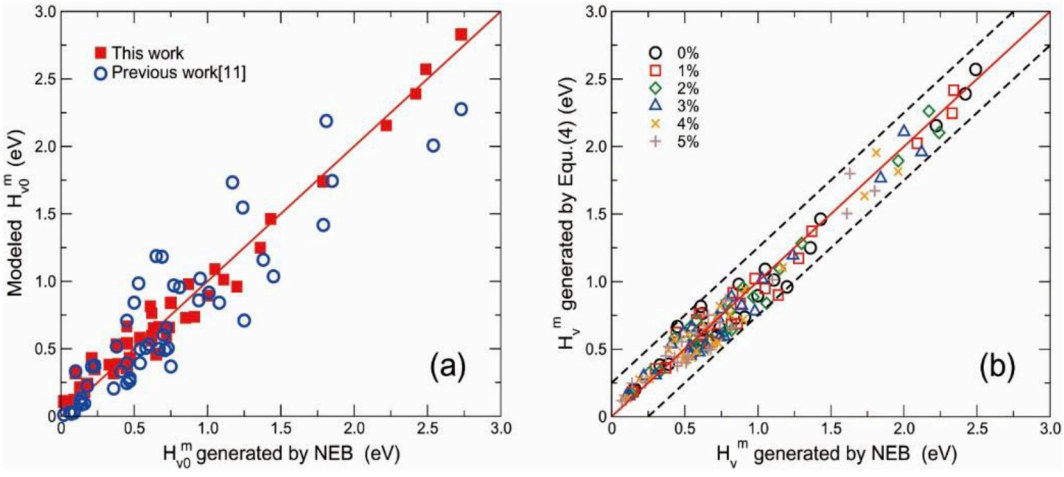

Fig. 5. (a) Modeled H_{v0}^m this work in filled squares and previous in open circles. (b) H_v^m versus DFT-NEB-derived data for all 24 fcc metals with the uniaxial strain.

a ratio as follow,

$$\lambda = \frac{r_{atom}}{L_{diagonal}} \quad (5)$$

where $L_{diagonal}$ is the diagonal length of the migration window and r_{atom} is the metallic radius of migrating atom. This ratio (λ) can be considered as the measure of the relative size of the migrating atom and the migration window. When the area of the migration window is much larger than that of migration atom, the atom will easily diffuse through this window. Within this situation, the atomic interaction bonding imposed by migration window is relatively weaker on the migrating atom. Therefore, it can be easily understood that the higher ratio λ is, the more difficult for atom to pass through the migration window. When the self-diffusion atom locates at the initial position (IS), for different fcc metals under the same degree of uniaxial strain, the value of λ is extremely close to each other (see details in (Supplementary Material). For instance, the λ of these ideal strain-free fcc metals is $1/\sqrt{6}$ for all 24 fcc metals. Once atom diffuses through this migration window along the *P1* path, its surrounding atom will experience the expansion reinforced by the diffusive atom, as illustrated in the right panel of Fig. 1. The atomic diffusion along the *P1* path from the IS to the TS could be in analogy with the situation of the applied compression along the *P1* path. Within such a process, the migration window tends to expand in the direction that perpendicular to the atom diffusion direction (see Fig. 1b, right panel). The local ε_x is the axial compression and both the local ε_y and ε_z are transversally expanded. Therefore, the physical meaning of the Poisson's ratio ν in Eqs. (2) and (4) can be understood as a specific value of the transversal expansion over the axial compression. As the axial compression of ε_x for atom locally migrating from the IS to the TS in *P1* is always $\sqrt{2}a/4$ even for fcc metals under uniaxial strain (a is the lattice constant of fcc metals that perpendicular to the uniaxial deformation). Hence, it is reasonable to expect that the higher value of ν reflects the larger expansion of the migration window, which results in the lower ratio λ. Based on the fact that the easier for the migrating atom to pass through the migration window, the lower H_v^m would be, it is safe to say that the value of H_v^m is proportional to the $1/\nu$. As a result, the synthetic effects of V_0B_0 and $1/\nu$ would be a good reason as to why the H_v^m can be expressed as a function of the product of V_0B_0/ν, as evidenced in Eqs. (2) and (4).

In order to verify the derived Eq. (4), we doubly checked 47 ground-state stable or metastable fcc elemental solids in two groups. As shown in Table 5, in Group I (Ag–Zr), we have predicted the H_{v0}^m at the ideal strain-free lattice ($\delta = 0$) for 24 fcc metals via our DFT-derived basic parameters of B_0, V_0 and ν. The modeled results are in good agreement with our currently DFT-NEB-derived data with the maximum deviation of 0.24 eV for fcc Ni and 0.23 eV for metastable fcc Ti. In Group II(Ac–Y), we have predicted the strain-free H_{v0}^m (with $\delta = 0$) for the other 23 fcc elemental solids through the derived Eq. (4) with the already published data of B_0, V_0 and ν in literatures [8,11]. In comparison with the previous DFT-NEB-derived data [11], the currently predicted values exhibit a highly good agreement, along with the maximum deviation of 0.22 eV for both metastable fcc La and Tl. Fig. 5a compiles the comparison between our currently modeled results and DFT-NEB-derived data for strain-free H_{v0}^m of 47 fcc elemental data. It can be seen that our current predictions for these 47 candidates indicates a much higher accuracy, as compared with the previous work [11]. It needs to be emphasized that for Th metal, our current modeling yields a H_{v0}^m value of 1.09 eV, in a good agreement with our current DFT-NEB-derived value of 1.05 eV and also with the previously published DFT- NEB-derived data (1.13 eV and 1.2 5eV) [3,11]. However, in comparison with the experimental estimation of 2.04 eV [7] for fcc Th, the current prediction shows an obvious deviation. As already discussed above, the possible reason for this exception of fcc Th may because by conventional computational DFT methods or by previous estimations of experiments, themselves. Furthermore, for Group I, we have predicted their strain-dependent $H_v^m(\delta)$ ($\delta =$ 0–0.05) for all 24 fcc ground-state stable or metastable metals.The resultant findings from Eq. (4) are plotted against the DFT-NEB-derived data in Fig. 5b. The solid red line in Fig. 5 represents the derived data exactly equals to DFT-NEB-derived data, whereas the dash lines define the range with the error deviation bar $\pm$ 0.25 eV. The data reproduced by Eq. (4) shows a highly nice agreement with the NEB-derived data. The Eq. (4)-generated values of over 60% fcc metals has the deviation within $\pm$ 0.1 eV from the DFT-NEB-derived data and for all 24 metals, the Eq. (4)-generated values fall into the deviation range within $\pm$ 0.25 eV.

4. Conclusions

Using first-principles calculations, we have investigated the diffusion behavior for vacancy in fcc metals under different degree of uniaxial tensile deformation. The obtained findings are two-fold.

The first finding is to develop a high-throughput, fast and effective model to derive the vacancy migration energy barrier via three fundamental material parameters of the equilibrium volume (V_0), the bulk modulus (B_0) and the Poisson's ratio (ν) for fcc elemental solids. This model is useful to the fcc lattice not only at the strain-free equilibrium state, but also at the uniaxial tensile strain. This model has provided enormous time efficiencies in computation, as compared with conventional DFT-NEB method. The accuracy of the model has been confirmed reasonable and acceptable verified by available experimental, published theoretical data, or new DFT-NEB-derived data.

The second finding is to investigate the effect of uniaxial tensile deformation on the diffusion behavior of vacancy in fcc metals. Through first-principles calculations, we have calculated the vacancy migration energy barriers for 24 fcc metals that under different degree of uniaxial tensile deformation (from 0% to 5%). The results demonstrate that in all 24 fcc metals, the energy barriers of vacancy migrate perpendicularly to the tensile deformation are obviously lower than those along the tensile direction as the uniaxial strain increases. These calculations reveal that the vacancy prefers to migrate to the direction that is perpendicular to the tensile deformation.

Acknowledgements

The work was supported by the National Science Fund for Distinguished Young Scholars (No. 51725103), by the National Natural Science Foundation of China (Grant Nos. 51671193 and 51474202), and by the Science Challenging Project No. TZ2016004. All calculations have been performed on the high-performance computational cluster in the Shenyang National University Science and Technology Park.

Appendix A. Supplementary data

Supplementary data to this article can be found online at https://doi.org/10.1016/j.pnsc.2019.02.007.

References

[1] H. Mehrer, Diffusion in Solids: Fundamentals, Methods, Materials, Diffusion-Controlled Processes, Springer, Berlin Heidelberg, 2007.
[2] P. Shewmon, Diffusion in Solids, second ed., The Minerals, Metals & Materials Society, Pittsburgh, 1989.
[3] S.L. Shang, B.C. Zhou, W.Y. Wang, A.J. Ross, X.L. Liu, Y.J. Hu, H.Z. Fang, Y. Wang, Z.K. Liu, Acta Mater. 109 (2016) 128.
[4] S.L. Shang, H.Z. Fang, J. Wang, C.P. Guo, Y. Wang, P.D. Jablonski, Y. Du, Z.K. Liu, Corros. Sci. 83 (2014) 94.
[5] A. Janotti, M. Krčmar, C.L. Fu, R.C. Reed, Phys. Rev. Lett. 92 (2004) 085901.
[6] P.T. Liu, S.L. Wang, D.Z. Li, Y.Y. Li, X.-Q. Chen, J. Mater. Sci. Technol. 32 (2016) 121.
[7] P. Ehrhart, P. Jung, H. Schultz, H. Ullmaier, Atomic Defects in Metal, Landolt-Börnstein, New Series, Group III vol. 25, Springer-Verlag, Berlin, 1991.
[8] E.A. Brandes, G.B. Brook, P. Paufler, Smithells Metals Reference Book, seventh ed., Butterworth-Heinemann, Oxford, 1992.
[9] G. Neumann, C. Tuijm, Self-Diffusion and Impurity Diffusion in Pure Metals: Handbook of Experimental Data, Elsevier, Oxford, 2011.
[10] R. Nazarov, T. Hickel, J. Neugebauer, Phys. Rev. B 85 (2012) 144118.

[11] T. Angsten, T. Mayeshiba, H. Wu, D. Morgan, New J. Phys. 16 (2014) 015018.
[12] B. Medasani, M. Haranczyk, A. Canning, M. Asta, Comput. Mater. Sci. 101 (2015) 96.
[13] H. Eyring, J. Chem. Phys. 3 (1935) 107.
[14] G.H. Vineyard, J. Phys. Chem. Solid. 3 (1957) 121.
[15] G. Henkelman, B.P. Uberuaga, H. Jonsson, J. Chem. Phys. 113 (2000) 9901.
[16] D. Sheppard, R. Terrell, G. Henkelman, J. Chem. Phys. 128 (2008) 134106.
[17] M.B. Manning, M.J. Moelter, C. Elbaum, Phys. Rev. B33 (1986) 1634.
[18] M. Militzer, W.P. Sun, J.J. Jonas, Acta Metall. Mater. 42 (1994) 133.
[19] K. Detemple, O. Kanert, J.T.M. Dehosson, K.L. Murty, Phys. Rev. B 52 (1995) 125.
[20] M. Lagos, H. Duque, Solid State Commun. 107 (1998) 311.
[21] U. Holzwarth, A. Barbieri, S. Hansen-Ilzhofer, P. Schaaff, M. Haaks, Appl. Phys. Mater. Sci. Process 73 (2001) 467.
[22] J. Schiotz, T. Leffers, B.N. Singh, Phil. Mag. Lett. 81 (2001) 301.
[23] T. Ungar, E. Schafler, P. Hanak, S. Bernstorff, M. Zehetbauer, Mat. Sci. Eng. A Struct. Mater. Prop. Microstruct. Process. 462 (2007) 398.
[24] V. Gavini, Phys. Rev. Lett. 101 (2008) 205503.
[25] D. Setman, E. Schafler, E. Korznikova, M.J. Zehetbauer, Mater. Sci. Eng. A-Struct. Mater. Prop. Microstruct. Process 493 (2008) 116.
[26] P. Hohenberg, W. Kohn, Phys. Rev. 136 (1964) B864.
[27] W. Kohn, L.J. Sham, Phys. Rev. 140 (1965) A1133.
[28] G. Kresse, J. Hafner, Phys. Rev. B 47 (1993) 558.
[29] G. Kresse, J. Furthmuller, Phys. Rev. B 54 (1996) 11169.
[30] P.E. Blöchl, Phys. Rev. B 50 (1994) 17953.
[31] J.P. Perdew, K. Burke, M. Ernzerhof, Phys. Rev. Lett. 77 (1996) 3865.
[32] R.E. Reed, H.R. Abbaschian, Physical Metallurgy Principles, PWS Engineering, Boston, 1973.
[33] D.P. Daroca, Solid State Commun. 252 (2017) 11.
[34] S.M. Kim, J.A. Jackman, W.J.L. Buyers, D.T. Peterson, J. Phys. F Met. Phys. 14 (1984) 2323.
[35] A. Glensk, B. Grabowski, T. Hickel, J. Neugebauer, Phys. Rev. X 4 (2014) 011018.
[36] W.W. Xing, P.T. Liu, X.Y. Cheng, H.Y. Niu, H. Ma, D.Z. Li, Y.Y. Li, X.-Q. Chen, Phys. Rev. B 90 (2014) 144105.
[37] A. Glensk, B. Grabowski, T. Hickel, J. Neugebauer, Phys. Rev. Lett. 114 (2015) 195901.
[38] J.F. Smith, O.N. Carlson, D.T. Peterson, T.E. Scott, Thorium: Preparation and Properties, Iowa State University Press, Ames, 1975.
[39] C.P. Flynn, Phys. Rev. 171 (1968) 682.
[40] O.H. Nielsen, R.M. Martin, Phys. Rev. Lett. 50 (1983) 697.
[41] Y. Le Page, P. Saxe, Phys. Rev. B 65 (2002) 104104.
[42] R. Hill, Proc. Phys. Soc. A 65 (1952) 349.
[43] H.M. Le, T.T. Pham, V.D. Dat, Y. Kawazoe, J. Phys. D Appl. Phys. 50 (2017) 035004.
[44] R.P. Vaningen, R.H.J. Fastenau, E.J. Mittemeijer, J. Appl. Phys. 76 (1994) 1871.
[45] S. Popovic, B. Grzeta, V. Ilakovac, R. Kroggel, G. Wendrock, H. Loffler, Phys. Stat. Sol. A 130 (1992) 273.
[46] M. Ellner, K. Kolatschek, B. Predel, J. Less Common. Met. 170 (1991) 171.
[47] G. Bruzzone, J. Less Common. Met. 25 (1971) 361.
[48] M. Singh, M. Barkei, G. Inden, S. Bhan, Phys. Stat. Sol. (a) 87 (1985) 165.
[49] F. Li, J. Yang, D. Xue, R. Zhou, J. Magn. Magn. Mater. 151 (1995) 221.
[50] A.E. Curzon, H.G. Chlebek, J. Phys. F Met. Phys. 3 (1973) 1.
[51] H.G. Smith, R. Berliner, J.D. Jorgensen, M. Nielsen, J. Trivisonno, Phys. Rev. B 41 (1990) 1231.
[52] J.W. Cable, Y. Tsunoda, J. Magn. Magn. Mater. 140 (1995) 93.
[53] A. Kumar, G. Chandra, O.P. Katyal, Phys. Stat. Sol. (a) 134 (1992) K9.
[54] Y. Sakamoto, F.L. Chen, R.A. McNicholl, J. Alloys Compd. 192 (1993) 145.
[55] S.N. Tripathi, M.S. Chandrasekharaiah, J. Less Common. Met. 91 (1983) 251.
[56] H.L. Luo, J.G. Huber, J. Less Common. Met. 65 (1979) 13.
[57] T.A. Badaeva, G.K. Alekseenko, Russ. J. Inorg. Chem. 4 (1959) 848 (Engl. Transl.).